

Diffusion-based Conditional ECG Generation with Structured State Space Models

Juan Miguel Lopez Alcaraz and Nils Strodthoff

Abstract—Synthetic data generation is a promising solution to address privacy issues with the distribution of sensitive health data. Recently, diffusion models have set new standards for generative models for different data modalities. Also very recently, structured state space models emerged as a powerful modeling paradigm to capture long-term dependencies in time series. We put forward SSSD-ECG, as the combination of these two technologies, for the generation of synthetic 12-lead electrocardiograms conditioned on more than 70 ECG statements. Due to a lack of reliable baselines, we also propose conditional variants of two state-of-the-art unconditional generative models. We thoroughly evaluate the quality of the generated samples, by evaluating pretrained classifiers on the generated data and by evaluating the performance of a classifier trained only on synthetic data, where SSSD-ECG clearly outperforms its GAN-based competitors. We demonstrate the soundness of our approach through further experiments, including conditional class interpolation and a clinical Turing test demonstrating the high quality of the SSSD-ECG samples across a wide range of conditions.

Index Terms—Cardiology, Electrocardiography, Signal processing, Synthetic data, Diffusion models, Time series.

I. INTRODUCTION

UNDoubtedly, the increased volume of data produced around the world has been one of the driving forces behind the tremendous advances in machine learning across many different data modalities and application domains. However, obtaining and distributing data can be difficult even across different departments within the same organization due to privacy concerns, in particular in privacy-critical domains such as healthcare [1], [2]. There has been an immense work around the improvement of security and privacy ecosystem for healthcare data, ranging from data privacy regulators such as the GDPR or HIPAA, and other works in regards to compliance [3]–[5], and with the development of technical solutions [6], [7]. However, also technical solutions such as federated learning as stand-alone solutions do not ensure full privacy protection, e.g., due to the possibility of reconstructing training samples from trained models through model inversion attacks [8], and hence combinations of different privacy-enhancing techniques have to be used.

The ability to create synthetic so-called digital twins of raw data, which preserve similar statistical features while discarding patients' personal information, represents such a

Juan Miguel Lopez Alcaraz and Nils Strodthoff are with the University of Oldenburg, 26129 Oldenburg, Germany (e-mail: juan.lopez.alcaraz@uol.de, nils.strodthoff@uol.de).

solution component. Statistical methods such as data augmentation aim to obfuscate the original data but provide only limited privacy protection. Therefore, generative machine learning models have recently become popular for the task. However, one must ensure a correct data recreation, otherwise, the data might suffer from bias [9], thus, leading to sub-optimal impact on downstream tasks and decisions, including interpretability [10]. This urges for generative models that are capable of generating high-quality samples conditioned on various patient characteristics but at the same time for the development of thorough benchmarking criteria to objectively assess the quality of the generated samples.

Lately, diffusion models have shown outstanding results for data synthesis, overcoming other generating modeling paradigms such as generative adversarial networks (GANs) or autoregressive models, which have shown biases towards high-density classes [11], [12], and towards low fidelity data-set distributions [13], [14], apart from known training instabilities [15]. In addition, diffusion models have provided improvements on further downstream tasks [16], and helped with the discovery of new pathologies [17].

In this work, we focus on the generation of synthetic electrocardiogram (ECG) data. The ECG is one of the most widely used medical procedure and is due to its non-invasive nature, reliance on only comparably simple and hence robust technology, and high diagnostic value an indispensable diagnostic tool for the first-in-line assessment of the overall cardiac state of a patient. This is even more true in the light of the recent advances in AI-based ECG analysis, see [18] for a recent perspective. However, most of the recent high-impact studies in the field of ECG analysis were established on private datasets, which represents a serious issue in terms of reproducibility and hampers the progress of the research community as a whole. The ability to generate high-quality digital twins of such datasets, which contain a lot of extremely sensitive patient data and therefore stand for very good reasons under very high privacy requirements, could enable the sharing of such datasets. We exemplify this process by creating and benchmarking synthetic copies of the PTB-XL dataset [19]–[21], a popular publicly accessible ECG dataset.

The primary contributions of this work are as follows: (1) We put forward a diffusion model for the generation of short (10s) 12-lead ECGs, which uses a structured state space model as internal model component. (2) We present conditional variants of two state-of-the-art unconditional GAN-based generative models for ECG data (3) We generate synthetic twins of PTB-XL, a large publicly available ECG dataset, and use

classifier performance trained/evaluated on these datasets to assess the quality of the generated samples. (4) We demonstrate that our model has internalized domain knowledge (a) by comparing generated samples using a beat-level aggregation across subgroups of samples with common pathologies (b) by meaningfully interpolating between different sets of conditions and (c) by performing an expert assessment in the form of a clinical Turing test confirming the high quality of the generated samples.

II. MATERIALS & METHODS

A. Dataset and downstream task

This work focuses on short (10s) 12-lead ECGs, as collected from six limb and six precordial leads, which corresponds to the most frequently encountered clinical setting. We work at a sampling rate of 100 Hz as prior work showed no significant improvement in predictive performance for standard ECG classification task when using higher sampling rates such as 500 Hz [22].

PTB-XL dataset: We base our experiments on the PTB-XL dataset [19]–[21], which is a large, publicly available ECG dataset of clinical 12-lead ECG comprising 21837 records from 18885 patients. Having a dataset of sufficient nominal size is the first prerequisite for training a high-quality generative model. For training class-conditional generative models, one requires, similar to supervised discriminative training, sample-wise annotations for all samples in the dataset. Also in this respect, PTB-XL represents a good choice as it provides annotations for each sample in terms of 71 ECG statement in a multi-label setting, covering a broad range of diagnostic statements over form-related statements to rhythm-related statements. It is worth stressing that it represents a significant advancement in terms of complexity to consider such a broad set of 71 ECG statements, which can even be used as multi-labels, as literature approaches mostly restricted themselves to just a single condition, i.e., typically healthy samples, or to generate samples conditioned on very restricted sets of (single-labeled) class labels. Further details on the dataset can be found in App. I.

Downstream task: As downstream task, we consider ECG statement prediction problem at the most fine-grained level of the 71 ECG statements mentioned above framed as a multi-label classification problem. This represents a well-studied benchmark task on the PTB-XL dataset and we follow the commonly used methodology established in prior work [23]. In particular, we report the macro-averaged area under the receiver operating curve (macro AUROC) across all 71 labels evaluated on the PTB-XL test set. As model architecture for the downstream task, we consider a XResNet50 model as proposed in [23], which is a one-dimensional adaptation of a modern ResNet model [24]. The training and evaluation methodology closely follow the description in [23]. The training objective is binary crossentropy loss as appropriate for a multi-label classification problem. The model is trained on random crops of 2.5s length. During test time, seven overlapping predictions from the same sample are averaged to obtain the final sample-wise prediction. We use the validation

set (macro AUROC) score for model selection. Further details on the downstream classifier and training can be found in App. II.

B. Background

Diffusion models: Diffusion models [25] are a subset of generative models that have shown state-of-the-art performance on a variety of data modalities, including audio data [26], [27], image data [13], [28]–[30], and video data [31]. A diffusion model consists of two processes, the forward process, during which noise is consecutively introduced in a Markovian manner, and the backward process, where the model is to gradually remove the noise. The forward process is parameterized as

$$q(x_1, \dots, x_T | x_0) = \prod_{t=1}^T q(x_t | x_{t-1}), \quad (1)$$

where $q(x_t | x_{t-1}) = \mathcal{N}(x_t; \sqrt{1 - \beta_t} x_{t-1}, \beta_t \mathbb{1})$, β_t are (fixed or learnable) forward-process variances, which adjust the noise level and T is the number of diffusion steps. Equivalently, x_t can be expressed in closed form as $x_t = \sqrt{\alpha_t} x_0 + (1 - \alpha_t) \epsilon$ for $\epsilon \sim \mathcal{N}(0, \mathbb{1})$, where $\alpha_t = \sum_{i=1}^t (1 - \beta_i)$. The backward process is parameterized as in Eq. (2), where $x_T \sim \mathcal{N}(0, \mathbb{1})$.

$$p_\theta(x_0, \dots, x_{t-1} | x_T) = p(x_T) \prod_{t=1}^T p_\theta(x_{t-1} | x_t) \quad (2)$$

Using a particular parameterization of $p_\theta(x_{t-1} | x_t)$, it was shown in [28] that the reverse process can be trained using

$$L = \min_\theta \mathbb{E}_{x_0 \sim \mathcal{D}, \epsilon \sim \mathcal{N}(0, \mathbb{1}), t \sim \mathcal{U}(1, T)} \|\epsilon - \epsilon_\theta(\sqrt{\alpha_t} x_0 + (1 - \alpha_t) \epsilon, t)\|_2^2, \quad (3)$$

where $\epsilon_\theta(x_t, t)$ is parameterized using a neural network and \mathcal{D} denotes the data distribution. This objective can be understood as a weighted variational bound on the negative log-likelihood that reduces the significance of terms at low t , i.e., at low noise levels. Class-conditional diffusion models can be realized by conditioning the backward process on desired set of labels c , i.e., using $\epsilon_\theta = \epsilon_\theta(x_t, t, c)$.

Structured state space models: Fundamentally, structured state space models (SSSMs) are based on a linear state space transition equation, which connects a one-dimensional input sequence $u(t)$ to a one-dimensional output sequence $y(t)$ through a N -dimensional hidden state $x(t)$,

$$\begin{aligned} x'(t) &= Ax(t) + Bu(t) \\ y(t) &= Cx(t) + Du(t). \end{aligned} \quad (4)$$

where A, B, C, D are transition matrices. The recently developed SSSM introduced in [32] represent a very promising modeling paradigm to capture long-term dependencies in time series, where after discretization, the relation between input and output can be written as a convolution operation, which can be evaluated effectively on modern GPUs using a custom kernel [32]. The ability to capture long-term dependencies is intimately related to a particular initialization of the hidden-to-hidden transition matrix A [33]. By stacking multiple copies of

such SSSM blocks with appropriate normalization and point-wise fully-connected layers in the manner of a transformer layer, one can construct a Structured State Space Sequence model (S4), which showed outstanding performance on a range of long-range-interaction benchmarks and a broad range of sequence classification tasks [32] including 12-lead ECG classification, as demonstrated most recently in [22].

Related work: Deep generative modeling for time series data is an emerging subfield in machine learning, which is mainly driven by the steady advances in the development of generative models, most notably in the imaging domain. While there have been developed diverse algorithms architectures such as variational autoencoders [34], and stacked denoising autoencoders [35], generative adversarial networks (GANs) is at the moment still represent the dominating technology in the field, specifically with RNNs as a building blocks [36]–[39], transformers [40], or differential equations [41]. Although some prior works addressed conditional time-series generation [34], [37], [39], [41], [42], most of them still remains restricted to the unconditional setting [36], [38], [40], [43], which severely limits their domain of applicability.

There have been various literature approaches addressing the problem of generating synthetic ECG signals. However, these literature works are subject to a number of major limitations: Firstly, many models only generate time series of short length [38]–[40], [43], secondly, they are often trained on training sets from very few patients [37] or small label sets in the conditional case [34], [41], [42], thirdly, many rely on the implementation of ECG beats segmentation as a preprocessing step rather than allow to work on continuous signals directly [34], [39]–[41] and, finally, many show different evaluation issues such as the restriction to patient-specific generation and classification [42] or the unavailability of training data as well as software for filtering/feature extraction for the general public [36]. We believe that fixing the training dataset to a public available ECG dataset is a crucial step for measurable progress as it otherwise remains impossible to disentangle improvements in model architecture or training schedule from improvements merely due to larger or more comprehensive training datasets. In contrast to the above limitations of prior work in the field, SSSD-ECG generates long sequences (1000 time steps for a 10s ECG at 100 Hz), is trained on a large dataset with more than 18k patients and conditioned on a rich set of annotation in terms of 71 ECG statements, generates full samples without prior segmentation or any other kind preprocessing and builds on publicly available code [44].

C. Conditional generative models for ECG data

SSSD-ECG: Coming back to the discussion of probabilistic diffusion in Sec. II-B, the remaining component that remains to be specified is the explicit parameterization of the backward process, i.e., $\epsilon_\theta = \epsilon_\theta(x_t, t, c)$. Here, we implement an adaption of the recently proposed $SSSD^{S4}$ model [45]. It, in turn, builds on the DiffWave architecture [27], which is a diffusion model proposed in the context of audio synthesis. $SSSD^{S4}$ replaces the dilated convolutions in the DiffWave model by two S4 layers, see Sec. II-B, for improved handling of long-term

dependencies in time series. This was demonstrated in [45] for different time series imputation and forecasting tasks. The information c to condition on is in this case the set of annotated ECG statements, encoded as a binary vector of length 71. This vector is transformed into a continuous representation to be used as conditioning information in the different $SSSD^{S4}$ layers by multiplying it by a learnable weight matrix. More details of the model internals and hyperparameters can be found in App. III.

As a final remark, it is important to note that only two of the six limb leads in a standard 12-lead ECG are independent, i.e. the full set of limb leads can be reconstructed from any given pair of limb leads by invoking the defining relations $III = II - I$, $aVL = (I - III)/2$, $aVF = (II + III)/2$, $-aVR = (I + II)/2$. In order to generate ECGs that satisfy these relations by construction, we train generative models to synthesize only 8 leads, the 6 precordial leads and 2 limb leads (I and aVF in our case), and reconstruct the remaining 4 leads after sampling from the two limb leads leads I and aVF. A similar approach was taken by [36] and is applied similarly also for all baseline models described below.

Baselines: WaveGAN* and Pulse2Pulse: Although our main model contribution is SSSD-ECG, we also propose a conditional versions of WaveGAN* and Pulse2Pulse [36], two generative models proposed for ECG data in the literature based on Generative Adversarial Networks (GANs) [46]. We turn these models class-conditional by introducing batch normalization layers in their architectures and subsequently turning these batch normalization layers into conditional batch normalization layers [47], where the layer’s internal shift and scaling parameters are rendered class-dependent. Here we follow a similar approach of mapping the binary label vector into a continuous representation through multiplication with a learned weight matrix. All model configurations and training hyperparameters are described in App. IV.

Unfortunately we were unable to train usable (even unconditional) generative models for our use case based on publicly available implementations apart from WaveGAN* and Pulse2Pulse mentioned above. This failure includes generative models for time series generation such as TTS-GAN [40] and even well-established methods such TimeGAN [43], which were most likely challenged by input lengths of 1000 time steps but we did also not succeed to generate samples at 250 time steps. Similarly, we were not able to train a class-conditional model based on the cVAE-ECG [34] approach, see App. IV-C for details.

III. EXPERIMENTS AND RESULTS

For each of the three proposed generative models, SSSD-ECG, WaveGAN* and Pulse2Pulse, we train a model based on the 8 PTB-XL training folds conditioned on the respective sample annotations in the dataset. For each of them, we then generate a synthetic copy of the PTB-XL dataset in the following manner: For each sample in PTB-XL, we generate a new synthetic sample by conditioning on the sample’s ECG annotation. This leads to three synthetic ECG datasets that precisely match PTB-XL in terms of nominal size as well as

label distribution. These datasets form the basis for qualitative and quantitative assessments of the quality of the generated samples.

A. Qualitative assessment

For the qualitative assessment, we select two frequently encountered conditions, NORM and LVH, and pick the 100 samples for which a classifier trained on real samples achieves the highest output probabilities (for the respective class). This step selects the most typical samples for the given condition. In order to be able to compare across samples, we perform a beat-level segmentation by identifying R-peaks and cropping from 300ms before the R-peak until 500ms after the R-peak. Now, we plot the median across all beats along with the corresponding 0.25 and 0.75 quantiles visualized through a shaded band, we also display a baseline of voltage 0 with a dashed line on each plot for comparison reference. This allows for a simple visual comparison of the main characteristics of the generated samples (across different models and in comparison to the real samples from PTB-XL).

Fig. 1 contains a qualitative assessment of healthy (NORM) generated samples in comparison to real samples. In contrast to the real samples, WaveGAN* contains a lot of inference in all of the signals, as well as different ECG features such as a larger R-peak, and absent P- and T-waves in most of the leads due to signal inference. The Pulse2Pulse model is more certain to its generations as there is a less variability across quantiles, however, in contrast to real samples, there are certain miss matched features, such as the missing S-peak in lead I, a larger S-peak in II, and an opposite (upwards) T-wave in V1. SSSD-ECG, however, is the model that more closely relate to the real samples, including a higher level of confidence as the quantile bands closely approximate to the median in all the features, such as the correct P- and T-waves in I and II, the correct T-wave (downwards) in V1, and balanced features in V2 such as R- and S-peaks, and P- and T-waves.

Fig. 2 contains a qualitative assessment of synthetic samples with left-ventricular hypertrophy (LVH) for the different proposed models in comparison to real samples. In contrast to the real samples, WaveGAN* has a lot of signal inference that prevents the observation of features such as P- and T-waves, though the R-peak seems to have a correct shape. On the other hand, the Pulse2Pulse model fails to correctly generate the R-peak, as it appears with a curved shape towards the top for all of the presented leads, and similarly, it fails to generate the most of the features, e.g., the T-wave is straight in V5 and downwards in V6 with a large amount of uncertainty. Finally, SSSD-ECG plots demonstrate the closest alignment against the real samples; it generates a correct R-peak with rather short P-waves and balanced T-waves for all beats with a steady confidence interval across all the presented leads.

To summarize, this first qualitative assessment already provides hints for the superiority of the SSSD-ECG samples

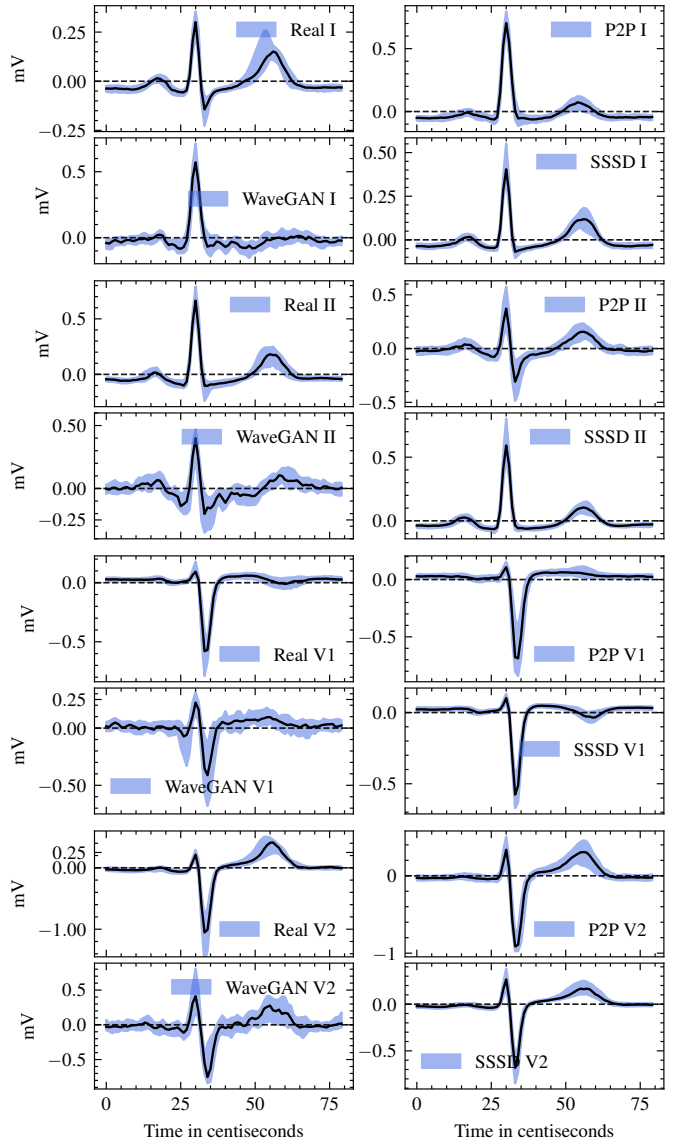


Fig. 1. From top to bottom four grids of leads I, II, V1, and V2 respectively, where for each grid from top to bottom and left to right real, WaveGAN*, Pulse2Pulse, and SSSD-ECG Median (black line) and 0.25-0.75 quantiles (blue shaded area) segmented beats for healthy (NORM) samples.

compared to its competitors and is in good accordance with the characteristics of the corresponding real samples from PTB-XL.

B. Quantitative assessment

In this section, we aim to quantify the hints on the quality of the generated samples acquired in the previous section. Given the synthetic copies of the full PTB-XL dataset, we can also quantitatively compare between the three generative models, which constitutes the heart of our study. In particular, we can now train classifiers on either real or synthetic training sets and evaluate them on either real or synthetic test sets. Note that it is sufficient to train a single classifier on real data, henceforth referred to as reference classifier, which is kept fixed for all the

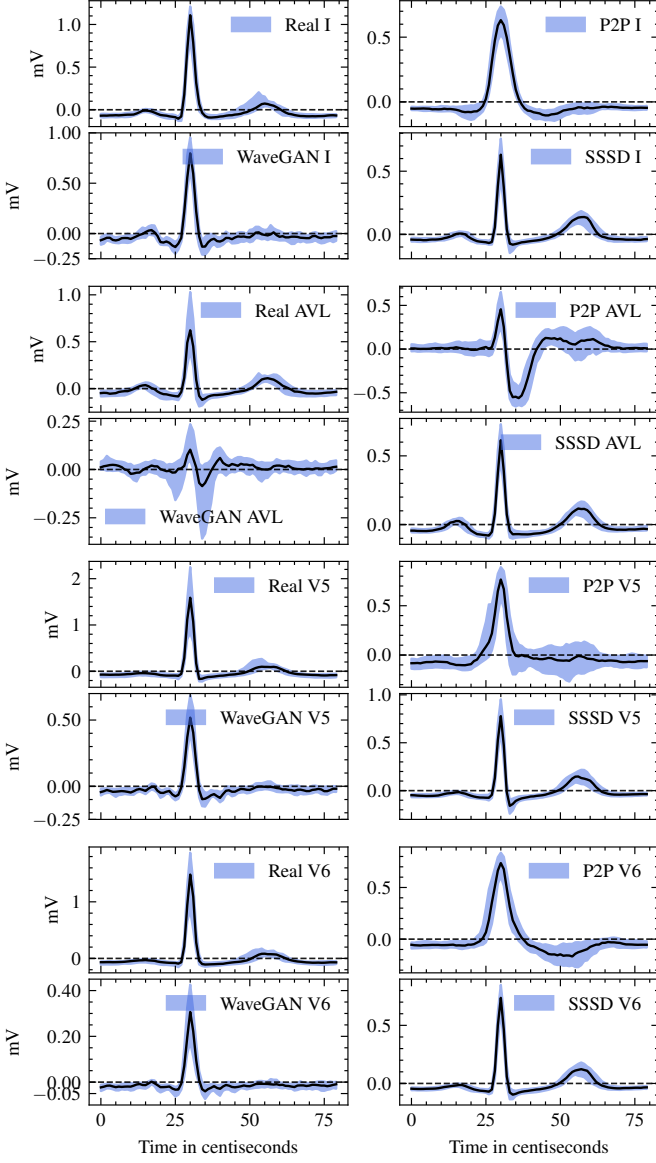


Fig. 2. From top to bottom four grids of leads I, AVL, V5, and V6 respectively, where for each grid from top to bottom and left to right real, WaveGAN*, Pulse2Pulse, and SSSD-ECG Median (black line) and 0.25-0.75 quantiles (blue shaded area) segmented beats for left-ventricular hypertrophy (LVH) samples.

remaining experiments. From it one can infer three different performance measures:

- 1) The first performance measure for synthetic data is its *ability to serve as a replacement for real data*. This is assessed by evaluating a classifier trained on a synthetic training set on the real test set. The ranking of different algorithms according to this criteria is widely considered as gold-standard for the assessment of the quality of model for synthetic data [48]. But also the absolute value set into perspective with the performance of the reference classifier evaluated on real data is of interest.
- 2) The second, complementary metric asks the question *how realistic is the synthetic data assessed by the reference classifier*. This is assessed by taking the reference

model trained on real data and evaluating its performance on the synthetic test set. The presumable drop in predictive performance compared to evaluation on the real test set caused by the inevitable mismatch between real training and synthetic test distribution can be used as second measure for the performance of generative models.

- 3) The third performance indicator follows a different pattern and assesses the *internal consistency* in the sense that for a given label combination there is a consistent imprint on the generated signals that generalizes across samples with this label combination. This can be assessed by evaluating a classifier trained on a synthetic training set on its corresponding synthetic test set. However, this criterion does not make any reference to the real data (neither directly nor indirectly through the reference classifier trained on real data) and is therefore considered less informative than the first two criteria.

At this point, we would also like highlight recent works such as [48] on performance criteria for (unconditional) generative models, which, however, ultimately try to replicate a ground truth ranking as inferred from our first performance criterion. We encountered instability issues when training one-class embedding as a required step in [48], which turned out to have significant impact on the results, which is why we decided not to present the corresponding results here.

TABLE I
CLASSIFICATION PERFORMANCE OF XRESNET50 MODELS
TRAINED/EVALUATED ON DIFFERENT COMBINATIONS OF
REAL/SYNTHETIC DATA.

Model	AUROC	
	Test real	Test synth.
WaveGAN*	0.9317	0.6489
Train real	0.5816	0.9793
Pulse2Pulse	0.9317	0.7082
Train real	0.5968	0.9950
SSSD-ECG	0.9317	0.9434
Train real	0.8402	0.9822

The results of this experiment are compiled in Tab. I. According to the first metric, SSSD-ECG clearly dominates its competitors with a score of 0.84 compared to only 0.60(Pulse2Pulse) and 0.58(WaveGAN*). One explanation for this result might be the fact that Pulse2Pulse and WaveGAN* are both GAN-based approaches, which are known for focusing on selected nodes instead of covering the full distribution. Also the second metric shows a similar picture with clearly dominating SSSD-ECG (0.94) and clearly inferior Pulse2Pulse (0.71) and WaveGAN* (0.64). According to the third metric all three approaches achieve scores of 0.98 or higher, which clearly indicates that all three models show a high degree of internal consistency. To summarize, our results reflect a very clear quantitative advantage of SSSD-ECG over its GAN-based competitors. Below, we reflect in more detail on its quantitative performance and its implications:

On the one hand, quite remarkably, SSSD-ECG even

achieves a slighter better score (0.94) assessed through the reference classifier compared to evaluating the reference classifier on real samples. This is a promising perspective for auditing scenarios for ECG analysis algorithms where a pre-screening might be carried out with synthetic data before evaluating them on high-quality private test data.

On the other hand, it is worth noting that even the SSSD-ECG performance for training on synthetic and testing on real data shows a sizable gap to the performance of the reference classifier trained on real data (0.84 vs. 0.93). At this point it is worth stressing again the difficulty of the generation task. This is the first attempt to build a generative model conditioned on a broad set of 71 ECG statements. Also here one should not underestimate the fact that these 71 statements are used in a multi-label setting, i.e., the number of unique label combinations (including co-occurring conditions) is considerably higher, but is only a reflection of the complex reality of co-occurring diseases and disease states. Not only are some of the ECG statements already sparsely populated with less than 100 occurrences across the whole dataset, but this applies even more to co-occurring label combinations. We see it as a challenging but worthwhile challenge for the research community to develop methods to close the gap in the train on synthetic test on real scenario, which would eventually allow to use synthetic data essentially interchangeably with real data.

C. Conditional class interpolation

To demonstrate that the SSSD-ECG model has acquired meaningful domain knowledge we present different class interpolation studies. Note that by the nature of how the conditional information is inserted into the model, we are not constrained to binary vectors as conditioning information but can support arbitrary real vectors with values taken from the unit interval. Thus, we can interpolate between a condition A, specified by a binary annotation vector a , and condition B, specified via a binary annotation vector b , by conditioning on the convex combination $\alpha a + (1-\alpha)b$ for $\alpha \in [0, 1]$, where α is the relative weight put on condition A. Everything else, in particular the sample's initialization before the start of the diffusion process, is kept fixed. Varying α then allows to smoothly interpolate between both conditions. For visualization, we segmented the generated samples based on R-peaks and present only median beats extracted from the signal, which allows to easier recognize signal changes when interpolating from condition A to condition B. This is not only an interesting consistency check, but the ability to condition on non-binary labels opens the possibility of building more complex generative models that allow to incorporate the non-binary nature of disease states.

Inferior myocardial infarction: Fig. 3 contains the interpolation between a healthy normal sample (NORM) and an inferior myocardial infarction (IMI) signal for lead V1. The labels combination based on training sample occurrence for healthy samples represent NORM, and sinus rhythm (SR), as well as SR, IMI, and abnormal QRS complex (ABQRS) for the IMI disease. There can be observed that the generated IMI signals and its interpolations presents an early Q-wave formation,

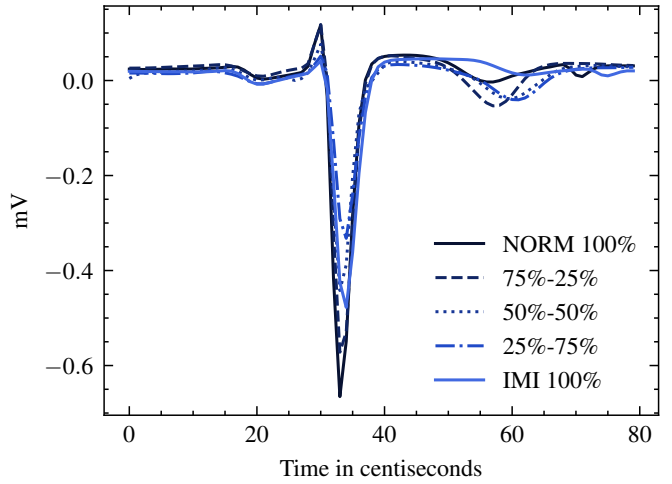


Fig. 3. SSSD-ECG interpolation between a healthy (NORM+SR) and an inferior myocardial infarction (IMI+SR+ABQRS) signal in lead V1, where 5 signals of 100% and 0%, 75%, and 25%, 50% and 50%, 25% and 75%, and 0% and 100% of healthy and inferior myocardial infarction, respectively.

while the normal signal presents a shorter and downward shape.

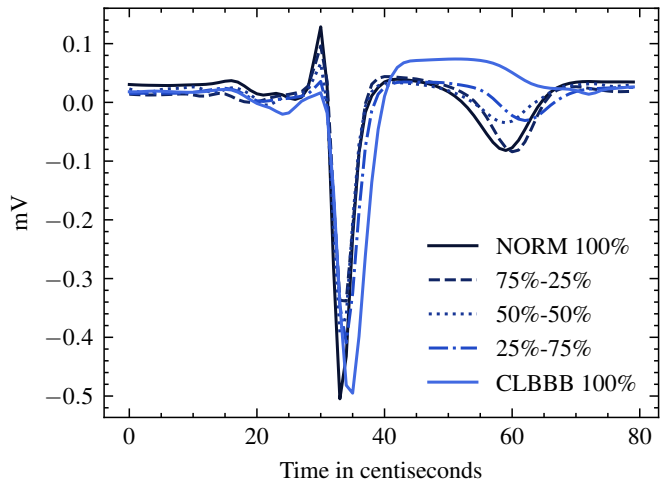


Fig. 4. SSSD-ECG interpolation between a healthy (NORM+SR) and a complete left bundle branch block signal (CLBBB+SR) in lead V1, where 5 signals of 100% and 0%, 75%, and 25%, 50% and 50%, 25% and 75%, and 0% and 100% of healthy and complete left bundle branch block, respectively.

Complete left bundle branch block: Fig. 4 contains the interpolation between a healthy and a complete left bundle branch block (CLBBB) signal as observed for lead V1. The labels combination based on training sample occurrence for healthy samples represent NORM, and SR, as well as SR, and CLBBB for the CLBBB disease. There can be observed diverse main features that more represent the CLBBB diseases in an ECG. Firstly, we can observe that the QRS complex is widened as the disease increase, clearly observed for the 75% and 100% CLBBB signals, secondly, there is observed on all the signals that as more the disease presents in the signal, the larger the RSR feature that is characteristic of it, lastly, we can

also observe an upwards trend on the T-wave as the disease increase.

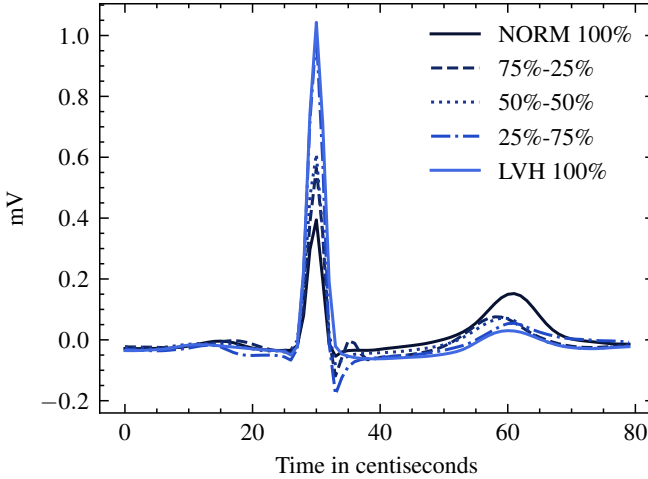


Fig. 5. SSSD-ECG interpolation between a healthy (NORM+SR) and a left ventricular hypertrophy signal (LVH+SR+VCLVH) in lead V5, where 5 signals of 100% and 0%, 75%, and 25%, 50% and 50%, 25% and 75%, and 0% and 100% of healthy and left ventricular hypertrophy, respectively.

Left ventricular hypertrophy: Fig. 5 contains the interpolation between a healthy and an left ventricular hypertrophy (LVH) signal as observed from lead V5. The labels combination based on training sample occurrence for healthy samples represent NORM, and SR, as well as SR, LVH and, voltage criteria (QRS) for left ventricular hypertrophy (VCLVH) for the LVH disease. There can be observed an important LVH ECG feature, which is the enlargement of the R-peak in one of the left-side leads (V5), clearly, as the disease increases, the R-peak also does, finally, there is also a downwards trend on the T-wave as the disease increase.

To summarize, these case interpolation studies across three different, which align with domain knowledge on the considered conditions, provide hints that SSSD-ECG has acquired a meaningful picture on how different label combinations relate to specific signal features.

D. Expert evaluation

As final component of our evaluation of the sample quality, we presented generated samples to an expert clinical and interventional cardiologist for qualitative assessment.

Generative diagnosis on normal samples: For this task, we presented four 10s 12-lead ECGs, one real and one sample from each of the generative models. The four full 10s ECGs provide an insightful visual picture of the generated samples. The expert was asked to decide if the signals were real or synthetic based on features in the series.

Figure 6 contains a 10 seconds of a real NORM signal, where the generative diagnosis by the medical expert was a synthetic sample due to changes in voltage in leads I, III, and AVF, as well as slow first vector (R-wave) progression thorough the precordial leads V1-V6. Figure 7 contains a 10 seconds of a WaveGAN* NORM signal, where the generative diagnosis by the medical expert was a real sample due to well defined P-wave, RR interval, and although there seems to be a bit of tachycardia it contains clear isodiphasic patterns, specially on I and AVF leads.



Fig. 6. Real (PTB-XL) NORM sample



Fig. 7. Synthetic WaveGAN* NORM sample

diagnosis by the medical expert was a synthetic sample based on no sinus signal, no clear P-wave, a lot of interference, no symmetry on RR intervals, and changes in voltage on the same trace. Figure 8 contains a 10 seconds of a Pulse2Pulse NORM signal, where the generative diagnosis by the medical expert was a synthetic sample due to variability in P-waves, no symmetry on RR intervals, a lot of inference, and morphological changes in the same trace within the same lead. Figure 9 contains a 10 seconds of a real NORM signal, where the generative diagnosis by the medical expert was a real sample due to well defined P-wave, RR interval, and although there seems to be a bit of tachycardia it contains clear isodiphasic patterns, specially on I and AVF leads.

Clinical Turing test: In this section, we present the results of a Turing test carried out with our already mentioned medical professional. The task involves the presentation of 22 pairs of



Fig. 8. Synthetic Pulse2Pulse NORM sample

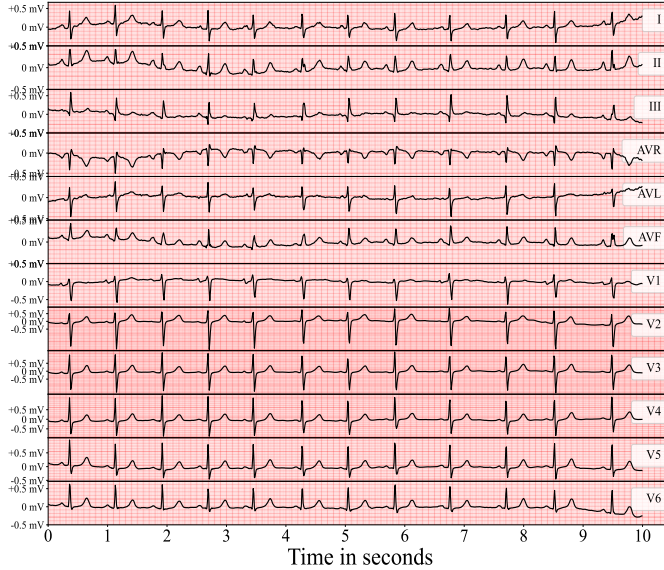


Fig. 9. Synthetic SSSD-ECG NORM sample

12-leads ECGs (44 total), where one is synthetic (22 total) and one real (22 total). The cardiologist was asked to perform two tasks: First, the aim was to decide if the sample was consistent with the provided set of ECG statements, which was either used to select a corresponding normal sample from PTB-XL or which was used to generate the synthetic sample. The second task involved to determine if any of the ECGs of the given pair seemed synthetic. In App. V, we present a detailed breakdown of the involved combinations, which correspond to the most frequent label combinations in PTB-XL, and the specific results for every pair, whereas we will only report simple descriptive statistics in this section. The original samples will be released as part of the code repository [44].

For the diagnosis samples evaluation as the first part of the assignment, out of the 44 total samples, cardiologist diagnosed

19 (43.18%) incorrectly, and 25 (56.81%) correctly, where from 22 synthetic samples, cardiologist diagnosed 7 (31.81%) incorrectly, and 15 (68.18%) correctly. Similarly, from the 22 real samples, cardiologist diagnosed 12 (54.54%) incorrectly, and 10 (45.45%) correctly. This even higher confirmation rate (68% vs. 45%) in the case of synthetic samples shows that the synthetic ECGs match their designated labels very well.

For the synthetic samples evaluation as the second part of the assignment, out of the 44 total samples, cardiologist identified 10 as synthetic (22.72%) and 34 as real (77.27%), where from the 22 synthetic samples, cardiologist identified 5 as synthetic (22.72%) and 17 as real (77.27%). Similarly, from the 22 real samples, cardiologist identified 5 as synthetic (22.72%) and 17 as real (77.27%). The fact that in both cases 5 samples were identified as synthetic confirms that real and synthetic samples are hardly distinguishable from the point of view of a medical expert. It is important to stress that this result holds across a very diverse set of 22 different conditions, again reinforcing the high quality of the generated samples.

IV. CONCLUSION

In this work we proposed SSSD-ECG as a diffusion-based approach for the generation of ECG data when conditioning a diverse set of 71 ECG statements in a multi-label setting, which represents an unprecedented degree of complexity. The generated samples excelled in different context from qualitative over quantitative evaluation based on deep ECG classifiers to conditional label interpolation and a human expert evaluation, clearly outperforming the two GAN-based competitors also proposed in this work. We still observe that the SSSD-ECG samples cannot fully compensate for real samples when training a classifier on them. We envision closing this gap as a worthwhile and measurable sign of progress in the field for the near future. To foster research in the field we release the source code underlying our investigations [44], trained models, as well as a synthetic copy of the PTB-XL dataset as generated by SSSD-ECG [49].

ACKNOWLEDGEMENTS

The authors express their deep gratitude to Erick Davila Zarazoga for the thorough assessment of the generated samples. Erick Davila Zaragoza is a clinical and interventional cardiologist certified by the Mexican national council of cardiology as a general practitioner from the University of Guadalajara (UDG), and as a cardiologist from the National Autonomous University of Mexico (UNAM).

APPENDIX I PTB-XL DATASET

Tab. II contains details on the PTB-XL dataset [19]–[21]. The PTB-XL ECG dataset consists of 21837 clinical 12-lead ECGs, each lasting 10 seconds, from 18885 patients. For all experiments, we collected the ECG signals at a sampling rate of 100 Hz. In all of the settings, the number of input channels is 12 as it is a 12 leads electrocardiogram. The PTB-XL dataset contains 21,837 samples for a full sample of 1,000 time steps (at signal length of 10s), where 17,441 samples are

for training, 2,193 for validation, and 2,203 for testing. The conditional information during the experiments carried out was the set of 71 possible labels in a multi-label setting.

TABLE II
PTB-XL DATASET DETAILS

Description	Value
Train set size	17,441
Validation set size	2,193
Test set size	2,203
Sample length	1000
Sample feature	12
Labels	71

APPENDIX II XRESNET50 DETAILS

Tab. III contains details on the XResNet(50) architecture, as proposed in [23], and the corresponding training hyperparameters. The model is composed of four blocks of 3, 4, 6, and 3 layers respectively of 1 dimensional convolutions with expansion of four and strides of 1. For training we utilize Adam as optimizer, learning rate and weight decay of 1×10^{-3} for 100 epochs and a batch size of 64. At difference than the generated ECG, we trained this classifier on cropped samples of 250 time steps each, and during inference time, we computed the mean output probabilities across seven different crops obtained by shifting the window through the signal using a stride of 125 time steps and used this mean output probability as prediction for the entire sequence.

TABLE III
XRESNET50 HYPERPARAMETERS

hyperparameter	Value
Block of layers	4
Layers in each block	[3,4,6,3]
Expansion	4
Stride	1
Optimizer	Adam
Learning rate	1×10^{-3}
Weight decay	1×10^{-3}
Batch size	64
Epochs	100

APPENDIX III SSSD-ECG DETAILS

Tab. IV contains details on the diffusion model SSSD-ECG, whose architecture is composed of a network of 36 stacked residual layers with 256 residual and skip channels. We refer the reader to [45] for an in-depth discussion of the model architecture. With a swish activation function over the second and third levels, SSSD-ECG has a three level diffusion embedding in 128, 256, and 256 dimensions. We constructed a convolutional layer after diffusion embedding to double the input's residual channel dimension and then compute the initial S4 diffusion. The deployment of a second S4 layer follows a similar increase of the conditional information and its inclusion to the input. The output is then routed through a gated-tanh as non-linearity, after which we use a convolutional layer

to project residual channels back to the channel dimensionality. As per hyperparameters, from a beta of 0.0001 to 0.02, we employed 200 time steps on a linear schedule for diffusion setup. Adam was used as an optimizer with a learning rate of $2e^{-4}$. In order to learn the temporal dependencies of series in both directions for the S4 model, we use a single bidirectional S4 layer. On the basis of earlier research [32], we use layer normalization and an internal state dimensionality $N = 64$.

TABLE IV
SSSD-ECG HYPERPARAMETERS

Hyperparameter	Value
Residual layers	36
Residual channels	256
Skip channels	256
Diffusion embedding dim. 1	128
Diffusion embedding dim. 2	512
Diffusion embedding dim. 3	512
Schedule	Linear
Diffusion steps T	200
B_0	0.0001
B_1	0.02
Optimizer	Adam
Loss function	MSE
Learning rate	2×10^{-4}
Batch size	4

APPENDIX IV BASELINE DETAILS

A. Pulse2Pulse details

Tab. V contains the architecture and training hyperparameters of the Pulse2Pulse implementation. Pulse2Pulse is similar to a U-Net architecture, however, using one-dimensional convolutional layers for the generation of ECG signals. The generator takes an input sampled from an uniform distribution of 1000 time steps and 8 channels, which passes through five down-sampling blocks and five up-sampling blocks, while the up-sampling is similar to the approach used in WaveGAN*, the down-sampling consist of a one-dimensional convolution and Leaky ReLU activation function. For the conditional setting, we added a conditional batch normalization at every convolution in the generator, which takes the batch of labels to condition which is passed through a word embedding with embedding dimension size of twice the output channel dimensions, then it is added to the convolution output.

TABLE V
PULSE2PULSE HYPERPARAMETERS

Hyperparameter	Value
Generator model size	50
Generator deconvolutional blocks	5
Discriminator model size	50
Discriminator convolutional blocks	6
Optimizer	Adam
Loss function	MSE
learning rate	0.0001
Training epochs	3000
Batch size	32

B. WaveGAN* details

Tab. VI contains the architecture and training hyperparameters of the WaveGAN* implementation. The generator input is a 1-dimensional vector of 1000 data points sampled from an uniform distribution, which passes through five deconvolution blocks to generate the desired output signal of 1000 time steps and 8 ECG leads. The deconvolution blocks were built from a series of four layers: an up-sampling layer, a padding layer, a 1D-convolution layer, and a ReLU activation function consecutively. Similarly, the discriminator and generator model size are 50 and 50 respectively. For the conditional setting, we added a conditional batch normalization at every convolution in the generator, which takes the batch of labels to condition which is passed through a word embedding with embedding dimension size of twice the output channel dimensions, then it is added to the convolution output.

TABLE VI
WAVEGAN* HYPERPARAMETERS

Hyperparameter	Value
Generator model size	50
Generator deconvolutional blocks	5
Generator latent dimensions	1000
Discriminator model size	50
Discriminator convolutional blocks	6
Optimizer	Adam
Loss function	MSE
learning rate	0.0001
Training epochs	3000
Batch size	32

C. Other baselines

Finally, we would like to comment on other baseline models for which we were not able to learn sensible generative models for our use case, namely TTS-GAN, TimeGAN and cVAE_ECG.

TTS-GAN [40], a GAN model for unconditional time series generations, was presented by their authors along with a diverse set of experiments, where one of them was for ECG generations, however, with an undefined segmentation of ECG signals at fixed time steps, aiming to extract clean ECG beats, at the cost of dropping continuous signals and signal length. We implemented TTS-GAN with diverse depth of layers for generator and discriminator such as 4, 6, 12, and 24, where for generator a latent dimension of 128, 256 and 1000. As our sequence length is 1000, we implemented mainly two settings, the first is a patch size of 200, and a embedding dimension of 5, the second consist of values 100 and 10 respectively. All the training on 200 epochs, batch size of 4, and learning rate of 0.0001 and 0.0003 for generator and discriminator respectively.

Similarly, TimeGAN [43] is a widely known GAN model for unconditional time series generation, which was implemented by their authors with a diverse set of experiments, however, most of them only on short signal lengths. We implemented TimeGAN model training with the default hyperparameters provided by the authors, such as 3 network layers of a GRU module, 24 hidden dimensions, with a batch size of

4 and 2000 training iterations, but failed to see any meaningful generated samples.

Variational autoencoders (VAEs) represent a popular framework for generative modeling. cVAE_ECG [34] was proposed as a conditional generative model specifically for ECG data. It differs from the approach followed in our work by the need to segment beats as data preprocessing as opposed to the generation of continuous signals in our work. Furthermore, the label set space of their implemented dataset is rather small. We used a learning rate of 0.001, batch size of 4, and diverse settings of convolutional filter dimension such as 3, 5, 8, and 10, similarly convolutional kernel at the length dimension of 10, 50, 100, 500, and 1000. Latent spaces of 10, 20, 50, 100, and 1000, where for all the settings a conditional dimensionality of 71 given the dataset labels. However, we failed to produce even reasonable reconstructions with the given model architecture.

APPENDIX V
CLINICAL TURING TEST: DETAILED RESULTS
BREAKDOWN

Tab. VII contains information about the diagnosis evaluation carried out as first part of the Turing test, where A(P), and B(P) are the predictions for sample A or B, respectively. The task was to confirm if the given set of labels match the represented sample or not. The value of true represents correct diagnosis whereas false represents incorrect diagnosis.

TABLE VII
TURING TEST DIAGNOSIS EVALUATION

Set	Labels	A(P)	B(P)
1	NORM, SR	True	False
2	NDT, SR	False	True
3	ABQRS, IMI, SR	True	False
4	NORM, SARRH	True	True
5	LAFB SR	False	True
6	NORM SBRAD	True	True
7	PACE	True	True
8	CLBBB, SR	True	False
9	LVH, SR, VCLVH	False	False
10	NORM	True	False
11	IRBBB, SR	True	False
12	ABQRS, NORM, SR	True	True
13	IRBBB, NORM, SR	True	False
14	NORM, STACH	False	True
15	IMI, SR	False	True
16	ISC-, LVH, SR	True	True
17	ABQRS, ASMI, SR	True	False
18	NST-, SR	False	True
19	NDT, NT-, SR	True	False
20	ABQRS, ASMI, IMI, SR	False	True
21	LVH, SR	False	False
22	AFIB, NST-	True	False

Tab. VIII contains information about the synthetic evaluation carried out as second part of the Turing test, where A(T), B(T), A(P), and B(P) denote the true label for sample A or B as well as the predicted labels for sample A or B, respectively. The value of true represents a synthetic sample whereas false represents a real sample.

TABLE VIII
TURING TEST SYNTHETIC EVALUATION

Set	Labels	A(T)	B(T)	A(P)	B(P)
1	NORM, SR	False	True	False	True
2	NDT, SR	False	True	False	False
3	ABQRS, IMI, SR	True	False	False	True
4	NORM, SARRH	True	False	False	False
5	LAFB SR	False	True	True	False
6	NORM SBRAD	True	False	False	True
7	PACE	False	True	False	True
8	CLBBB, SR	False	True	False	True
9	LVH, SR, VCLVH	False	True	False	True
10	NORM	True	False	False	False
11	IRBBB, SR	True	False	False	True
12	ABQRS, NORM, SR	True	False	False	False
13	IRBBB, NORM, SR	False	True	False	False
14	NORM, STACH	False	True	False	False
15	IMI, SR	True	False	False	False
16	ISC-, LVH, SR	False	True	False	False
17	ABQRS, ASMI, SR	True	False	False	False
18	NST-, SR	True	False	False	False
19	NDT, NT-, SR	True	False	False	False
20	ABQRS, ASMI, IMI, SR	False	True	False	True
21	LVH, SR	False	True	False	False
22	AFIB, NST-	True	False	False	True

REFERENCES

- M. Tzanou, *Health Data Privacy under the GDPR: Big Data Challenges and Regulatory Responses*, ser. Routledge Research in the Law of Emerging Technologies. Taylor & Francis, 2020.
- J. Sullivan and A. B. A. H. L. Section, *HIPAA: A Practical Guide to the Privacy and Security of Health Data*, ser. Hein's ABA Archive Microfiche Collection. Health Law Section, American Bar Association, 2004.
- A. Abbas and S. U. Khan, “A review on the state-of-the-art privacy-preserving approaches in the e-health clouds,” *IEEE Journal of Biomedical and Health Informatics*, vol. 18, pp. 1431–1441, 2014.
- J. L. Fernández-Alemán, I. C. Señor, P. Ángel Oliver Lozoya, and A. Toval, “Security and privacy in electronic health records: A systematic literature review,” *Journal of Biomedical Informatics*, vol. 46, no. 3, pp. 541–562, 2013.
- M. M. Farooqi, M. A. Shah, A. Wahid, A. Akhunzada, F. Khan, N. ul Amin, and I. Ali, *Big Data in Healthcare: A Survey*. Cham: Springer International Publishing, 2019, pp. 143–152.
- R. Kumar, W. Wang, J. Kumar, T. Yang, A. Khan, W. Ali, and I. Ali, “An integration of blockchain and ai for secure data sharing and detection of ct images for the hospitals,” *Computerized Medical Imaging and Graphics*, vol. 87, p. 101812, 2021.
- J. Xu, B. S. Glicksberg, C. Su, P. Walker, J. Bian, and F. Wang, “Federated learning for healthcare informatics,” *Journal of Healthcare Informatics Research*, vol. 5, no. 1, pp. 1–19, Nov. 2020.
- H. Yin, A. Mallya, A. Vahdat, J. M. Alvarez, J. Kautz, and P. Molchanov, “See through gradients: Image batch recovery via gradinversion,” in *Proceedings of the IEEE/CVF Conference on Computer Vision and Pattern Recognition*, 2021, pp. 16 337–16 346.
- P. Madley-Dowd, R. Hughes, K. Tilling, and J. Heron, “The proportion of missing data should not be used to guide decisions on multiple imputation,” *Journal of Clinical Epidemiology*, vol. 110, pp. 63–73, 2019.
- T. Shadbahr, M. Roberts, J. Stanczuk, J. Gilbey, P. Teare, S. Dittmer, M. Thorpe, R. V. Torne, E. Sala, P. Lio, M. Patel, A.-C. Collaboration, J. H. F. Rudd, T. Mirtti, A. Rannikko, J. A. D. Aston, J. Tang, and C.-B. Schönlieb, “Classification of datasets with imputed missing values: does imputation quality matter?” *arXiv preprint 2206.08478*, 2022.
- A. Brock, J. Donahue, and K. Simonyan, “Large scale gan training for high fidelity natural image synthesis,” *arXiv preprint 1809.11096*, 2018.
- V. Schwag, C. Hazirbas, A. Gordo, F. Ozgenel, and C. C. Ferrer, “Generating high fidelity data from low-density regions using diffusion models,” *arXiv preprint 2203.17260*, 2022.
- P. Dhariwal and A. Nichol, “Diffusion models beat gans on image synthesis,” in *Advances in Neural Information Processing Systems*, vol. 34, 2021, pp. 8780–8794.
- R. Child, S. Gray, A. Radford, and I. Sutskever, “Generating long sequences with sparse transformers,” *arXiv preprint 1904.10503*, 2019.
- A. M. Delaney, E. Brophy, and T. E. Ward, “Synthesis of realistic ecg using generative adversarial networks,” *arXiv preprint 1909.09150*, 2019.
- M. Seibold, A. Hoch, M. Farshad, N. Navab, and P. Fürnstahl, “Conditional generative data augmentation for clinical audio datasets,” *arXiv preprint 2203.1570*, 2022.
- K. Falahkheirkhah, S. Tiwari, K. Yeh, S. Gupta, L. Herrera-Hernandez, M. R. McCarthy, R. E. Jimenez, J. C. Cheville, and R. Bhargava, “Deepfake histological images for enhancing digital pathology,” *arXiv preprint 2206.08308*, 2022.
- E. J. Topol, “What’s lurking in your electrocardiogram?” *The Lancet*, vol. 397, no. 10276, p. 785, 2021.
- P. Wagner, N. Strothoff, R.-D. Bousseljot, D. Kreiseler, F. I. Lunze, W. Samek, and T. Schaeffter, “PTB-XL, a large publicly available electrocardiography dataset,” *Scientific Data*, vol. 7, no. 1, p. 154, 2020.
- P. Wagner, N. Strothoff, R.-D. Bousseljot, W. Samek, and T. Schaeffter, “PTB-XL, a large publicly available electrocardiography dataset,” 2020.
- A. L. Goldberger, L. A. N. Amaral, L. Glass, J. M. Hausdorff, P. C. Ivanov, R. G. Mark, J. E. Mietus, G. B. Moody, C.-K. Peng, and H. E. Stanley, “PhysioBank, PhysioToolkit, and PhysioNet,” *Circulation*, vol. 101, no. 23, pp. e215–e220, 2000.
- T. Mehari and N. Strothoff, “Advancing the State-of-the-Art for ECG Analysis through Structured State Space Models,” in *arXiv*, 2022, extended abstract.
- N. Strothoff, P. Wagner, T. Schaeffter, and W. Samek, “Deep learning for ecg analysis: Benchmarks and insights from ptb-xl,” *IEEE Journal of Biomedical and Health Informatics*, vol. 25, no. 5, pp. 1519–1528, 2021.
- T. He, Z. Zhang, H. Zhang, Z. Zhang, J. Xie, and M. Li, “Bag of tricks for image classification with convolutional neural networks,” in *Proceedings of the IEEE/CVF Conference on Computer Vision and Pattern Recognition*, 2019, pp. 558–567.
- J. Sohl-Dickstein, E. Weiss, N. Maheswaranathan, and S. Ganguli, “Deep unsupervised learning using nonequilibrium thermodynamics,” in *Proceedings of the 32nd International Conference on Machine Learning*, ser. Proceedings of Machine Learning Research, vol. 37, 07–09 Jul 2015, pp. 2256–2265.
- N. Chen, Y. Zhang, H. Zen, R. J. Weiss, M. Norouzi, and W. Chan, “Wavegrad: Estimating gradients for waveform generation,” in *International Conference on Learning Representations*, 2020.
- Z. Kong, W. Ping, J. Huang, K. Zhao, and B. Catanzaro, “Diffwave: A versatile diffusion model for audio synthesis,” in *9th International Conference on Learning Representations, ICLR 2021*, 2021.
- J. Ho, A. Jain, and P. Abbeel, “Denoising diffusion probabilistic models,” in *Advances in Neural Information Processing Systems*, vol. 33, 2020, pp. 6840–6851.
- J. Ho, C. Saharia, W. Chan, D. Fleet, M. Norouzi, and T. Salimans, “Cascaded diffusion models for high fidelity image generation,” *J. Mach. Learn. Res.*, vol. 23, pp. 47:1–47:33, 2022.
- R. Rombach, A. Blattmann, D. Lorenz, P. Esser, and B. Ommer, “High-resolution image synthesis with latent diffusion models,” in *Proceedings of the IEEE/CVF Conference on Computer Vision and Pattern Recognition*, 2022, pp. 10 684–10 695.
- J. Ho, T. Salimans, A. Gritsenko, W. Chan, M. Norouzi, and D. J. Fleet, “Video diffusion models,” *arXiv preprint 2204.03458*, 2022.
- A. Gu, K. Goel, and C. Ré, “Efficiently modeling long sequences with structured state spaces,” in *International Conference on Learning Representations*, 2022.
- A. Gu, T. Dao, S. Ermon, A. Rudra, and C. Ré, “Hippo: Recurrent memory with optimal polynomial projections,” in *Advances in Neural Information Processing Systems*, vol. 33, 2020, pp. 1474–1487.
- Y. Sang, M. Beetz, and V. Grau, “Generation of 12-lead electrocardiogram with subject-specific, image-derived characteristics using a conditional variational autoencoder,” in *2022 IEEE 19th International Symposium on Biomedical Imaging (ISBI)*, 2022, pp. 1–5.
- M. A. Rahhal, Y. Bazi, H. AlHichri, N. Alajlan, F. Melgani, and R. Yager, “Deep learning approach for active classification of electrocardiogram signals,” *Information Sciences*, vol. 345, pp. 340–354, 2016.
- V. Thambawita, J. L. Isaksen, S. A. Hicks, J. Ghouse, G. Ahlberg, A. Linneberg, N. Grarup, C. Ellervik, M. S. Olesen, T. Hansen, C. Graff, N.-H. Holstein-Rathlou, I. Strümke, H. L. Hammer, M. M. Maleckar, P. Halvorsen, M. A. Riegler, and J. K. Kanters, “DeepFake electrocardiograms using generative adversarial networks are the beginning of the end for privacy issues in medicine,” *Sci. Rep.*, vol. 11, no. 1, p. 21896, Nov. 2021.

[37] F. Zhu, F. Ye, Y. Fu, Q. Liu, and B. Shen, “Electrocardiogram generation with a bidirectional LSTM-CNN generative adversarial network,” *Scientific Reports*, vol. 9, 2019.

[38] A. M. Delaney, E. Brophy, and T. E. Ward, “Synthesis of realistic ecg using generative adversarial networks,” *arXiv preprint 1909.09150*, 2019.

[39] T. Golany, G. Lavee, S. Tejman Yarden, and K. Radinsky, “Improving ecg classification using generative adversarial networks,” *Proceedings of the AAAI Conference on Artificial Intelligence*, vol. 34, no. 08, pp. 13 280–13 285, Apr. 2020.

[40] X. Li, V. Metsis, H. Wang, and A. H. H. Ngu, “Tts-gan: A transformer-based time-series generative adversarial network,” in *Artificial Intelligence in Medicine*, M. Michalowski, S. S. R. Abidi, and S. Abidi, Eds. Cham: Springer International Publishing, 2022, pp. 133–143.

[41] T. Golany, K. Radinsky, and D. Freedman, “SimGANs: Simulator-based generative adversarial networks for ECG synthesis to improve deep ECG classification,” in *Proceedings of the 37th International Conference on Machine Learning*, ser. Proceedings of Machine Learning Research, H. D. III and A. Singh, Eds., vol. 119. PMLR, 13–18 Jul 2020, pp. 3597–3606.

[42] T. Golany and K. Radinsky, “Pgans: Personalized generative adversarial networks for ecg synthesis to improve patient-specific deep ecg classification,” *Proceedings of the AAAI Conference on Artificial Intelligence*, vol. 33, no. 01, pp. 557–564, Jul. 2019.

[43] J. Yoon, D. Jarrett, and M. van der Schaar, “Time-series generative adversarial networks,” in *Advances in Neural Information Processing Systems*, H. Wallach, H. Larochelle, A. Beygelzimer, F. d’Alché-Buc, E. Fox, and R. Garnett, Eds., vol. 32. Curran Associates, Inc., 2019.

[44] J. M. L. Alcaraz and N. Strodthoff, “SSSD-ECG public code repository,” <https://zenodo.org/account/settings/github/repository/AI4HealthUOL/SSSD-ECG>, accessed: 2022-12-31.

[45] ———, “Diffusion-based time series imputation and forecasting with structured state space models,” *arXiv preprint 2208.09399*, 2022.

[46] I. Goodfellow, J. Pouget-Abadie, M. Mirza, B. Xu, D. Warde-Farley, S. Ozair, A. Courville, and Y. Bengio, “Generative adversarial networks,” *Communications of the ACM*, vol. 63, no. 11, pp. 139–144, 2020.

[47] H. De Vries, F. Strub, J. Mary, H. Larochelle, O. Pietquin, and A. C. Courville, “Modulating early visual processing by language,” *Advances in Neural Information Processing Systems*, vol. 30, 2017.

[48] A. Alaa, B. Van Breugel, E. S. Saveliev, and M. van der Schaar, “How faithful is your synthetic data? Sample-level metrics for evaluating and auditing generative models,” in *Proceedings of the 39th International Conference on Machine Learning*, ser. Proceedings of Machine Learning Research, K. Chaudhuri, S. Jegelka, L. Song, C. Szepesvari, G. Niu, and S. Sabato, Eds., vol. 162. PMLR, 17–23 Jul 2022, pp. 290–306.

[49] J. M. L. Alcaraz and N. Strodthoff, “SSSD-ECG data repository,” <https://figshare.com/s/43df16e4a50e4dd0a0c5>, accessed: 2022-01-19.